

10th World Conference on Neutron Radiography 5-10 October 2014

## Imaging with Cold Neutrons at the CONRAD-2 Facility

Nikolay Kardjilov<sup>a\*</sup>, André Hilger<sup>a</sup>, Ingo Manke<sup>a</sup>, Axel Griesche<sup>b</sup>, John Banhart<sup>a</sup>

<sup>a</sup>*Helmholtz-Zentrum-Berlin, Hahn-Meitner-Platz 1, 14109 Berlin, Germany*

<sup>b</sup>*BAM Federal Institute for Materials Research and Testing, Unter den Eichen 87, 12205 Berlin, Germany*

---

### Abstract

CONRAD-2 is an imaging instrument using low-energy (cold) neutrons. The instrument is installed at the end of a curved neutron guide which avoids the direct line of sight towards the reactor core. This ensures a very low background of high-energy neutrons and  $\gamma$  photons at the sample position. The cold neutron beam provides a wavelength range which is suitable for phase- and diffraction-contrast imaging such as grating interferometry and Bragg edge mapping. The instrument is well suited for high resolution imaging due to the high efficiency of the very thin scintillators that can be used for the detection of cold neutrons. An instrument upgrade was performed recently as a part of an upgrade program for the cold neutron instrumentation at HZB. The parameters of the instrument as well as some research highlights will be presented.

© 2015 The Authors. Published by Elsevier B.V. This is an open access article under the CC BY-NC-ND license (<http://creativecommons.org/licenses/by-nc-nd/4.0/>).

Selection and peer-review under responsibility of Paul Scherrer Institut

Keywords: neutron imaging; neutron instrumentation; cold neutrons; iron embrittlement

---

### 1. General introduction and history

The imaging facility at the BER II reactor was designed in 2004 and constructed in 2005 as an instrument supporting the materials research activities at the Helmholtz-Zentrum Berlin (HZB) - formerly Hahn-Meitner-Institute (Kardjilov et al., 2011b). The name of the facility – CONRAD – stands for Cold Neutron Radiography. The CONRAD-1/V7 instrument was situated at the curved neutron guide NL-1B ( $^{58}\text{Ni}$ ) with a characteristic wavelength of 2.2 Å. This neutron guide served two other instruments in front of CONRAD-1: the reflectometer V14 and the triple-axis spectrometer FLEX/V2. The available space behind the neutron guide of ~5 m did not

---

\* Corresponding author. Tel.: +49-30-8062-42298; fax: +49-30-8062-43059.  
E-mail address: [kardjilov@helmholtz-berlin.de](mailto:kardjilov@helmholtz-berlin.de)

allow for a long collimation path. Therefore, the beam size at the sample position was limited to 10 cm × 10 cm due to the small divergence of the beam transported by the guide (Kardjilov et al., 2010; Tötzke et al., 2012). This size was quite small for conventional imaging purposes and was a competitive disadvantage to other existing facilities worldwide. This was the reason to concentrate on the development of novel methods (N. Kardjilov et al., 2011; Strobl et al., 2009) which benefit from the cold neutron beam and the low background at the instrument. Significant development work was performed to expand the radiographic and tomographic capabilities of the beamline. New techniques were implemented, including imaging with polarised neutrons (Kardjilov et al., 2008b; Manke et al., 2008), Bragg-edge mapping (Woracek et al., 2014; Woracek et al., 2011), high-resolution neutron imaging (Williams et al., 2012) and grating interferometry (Hilger et al., 2010; Manke et al., 2010; Strobl et al., 2008). These methods were provided to the user community as tools to help solving scientific problems in a broad range of topics such as superconductivity, materials research, life sciences, cultural heritage and palaeontology. Industrial applications (Manke et al., 2009) including fuel cell research (Klages et al., 2013; Schroder et al., 2013) have also been fostered by these new developments that have also helped to increase and improve the scientific output of the facility and to attract new users.

The instrument was included in a general upgrade program for the cold neutron instrumentation at HZB which was performed from October 2010 to October 2012. The upgrade included: i) an exchange of the  $^{58}\text{Ni}$ -based neutron guides ( $m=1.2$ ) by new supermirror guides ( $m=2.5$  and  $m=3$ ) and ii) an increase of the collimation path from 5 m to 10 m. The expected effects were to improve the efficiency of neutron transport and to increase the beam size due to a larger beam divergence and longer collimation path. Additionally, the curvature of the guide was increased in order to enlarge the distance from the shielding of the neighbouring instrument.

Following a commissioning period with neutrons from August 2012 the upgraded instrument named CONRAD-2 has been back to full user operation since October 2012 and the first user experiments have been successfully completed.

The expected intensity gain including the contribution from the exchange of the cold source by more efficient one has been confirmed to be a factor of 10 at the end of the guide (at the pinhole position) and a factor 2.4 at the sample position (at a distance 10 m from the pinhole at a defined L/D ratio). The obtained beam size now allows for investigating samples up to 30 cm × 30 cm directly (without scanning the sample which allows for going up to 50 cm × 50 cm). This corresponds to a gain of 4 in comparison to the previous configuration. New methods such as energy-selective imaging and grating interferometry will benefit from the increased neutron flux and better beam collimation as well.

### Nomenclature

$\rho$	density, $g/cm^3$ or $mol/m^3$
$\Sigma$	linear attenuation coefficient, $cm^{-1}$
$N_A$	Avogadro's constant, $mol^{-1}$
$\sigma_{total}$	total cross-section for neutrons, $barn$ or $10^{-24} cm$
<i>at.wt.</i>	atomic weight, $mol^{-1}$
$M$	molar weight, $g/mol$

## 2. Instrument parameters and scientific case

CONRAD-2 is a recently upgraded cold-neutron imaging instrument operating in the wavelength range between 1.5 Å and 6.0 Å (maximum at 2.5 Å). The instrument is installed at the end of a curved neutron guide with a characteristic wavelength of 1.8 Å. The supermirror coated guide ( $m=2.5$  for the inner wall and  $m=3.0$  for the outer, top and bottom walls) provides a divergent beam which gives rise to a beam size of 30 cm × 30 cm at the sample position located at a distance of 11 m behind the end of the guide. The neutron spectrum at the end of the guide is provided in Fig. 1.

CONRAD-2 is a low background instrument due to the curved neutron guide which blocks the direct view on the reactor core. The measured (gold foil) flux density at the sample position is  $2.4 \times 10^7$  n/cm<sup>2</sup>/s at L/D ratio of

350. The instrument is well suited for high-resolution imaging due to the high efficiency of the very thin scintillators used for cold neutrons and the very low background which reduces the noise (white spots) in images at long exposure times. Beam preparation options include a double-crystal monochromator and a velocity selector for energy-selective imaging, solid state polarised bender and polarised  $^3\text{He}$  spin filters for imaging with polarised neutrons, phase gratings for grating interferometry and, for detection, a high-resolution detector system (a prototype). The instrument parameters are summarised in Table 1.

Table 1: Instrument specifications and options

Neutron guide	NL-1A (m=2.5 and 3) with beam cross-section 125 mm (height) $\times$ 30 mm (width) radius of curvature 750 m
Pinhole exchanger	1 cm, 2 cm and 3 cm diameter
Flight path	10 m flight path Aluminium containers filled with He
Measuring positions	Position: end of the guide Flux: $2.6 \times 10^9$ n/cm <sup>2</sup> s @ L/D ca. 70; beam size: 12 $\times$ 3 cm  Position: high-resolution Flux: $7.2 \times 10^7$ n/cm <sup>2</sup> s @ L/D 170; beam size: 15 $\times$ 15 cm  Position: large samples Flux: $2.4 \times 10^7$ n/cm <sup>2</sup> s @ L/D 350; beam size: 30 $\times$ 30 cm
Double crystal monochromator	Pyrolytic graphite (002) with mosaicity of 0.8° Wavelength resolution 3% Wavelength range: 1.5 Å – 6.0 Å
Velocity selector	Wavelength range: 3.0 Å – 6.0 Å Wavelength resolution 10 – 20 %
Polarisers	2 Solid-state benders 4 Polarised $^3\text{He}$ cells and 2 magic boxes
Detectors	CCD camera (Andor CCD, 2048 x 2048 pixels) sCMOS camera (Andor Neo, 2560 x 2160 pixels)
Sample manipulator	Rotation table: 0-360° Translation table: 0-800 mm Lift table: 0-250 mm Maximum weight: 200 kg

The layout of the CONRAD-2 facility together with all components and their interaction is presented in Fig. 1. Two measuring positions for high-resolution and large samples are located in the middle and at the end of the beam path. The detector and sample environment of the high-resolution position can be translated out of the beam when measurements at the large sample position are performed, see Fig. 1. For some special cases which require high neutron flux (e.g. investigation for dynamic processes and high-speed tomography) the position at the neutron guide (neutron flux of  $2.6 \times 10^9$  n/cm<sup>2</sup>s @ L/D ca. 70) can be used. The devices double-crystal monochromator, source gratings and velocity selector are installed permanently at the facility and can be activated in a short time of few minutes. The neutron polarizer-analyzer equipment is available and can be installed at request.

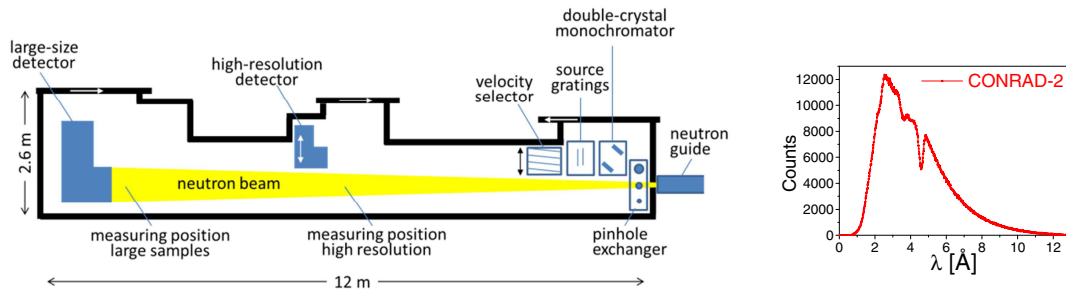


Fig. 1. Layout of the CONRAD-2 instrument (top view) with schematic representation of its components and their interaction on the left. The neutron spectrum measured by TOF method at the end of the neutron guide is shown on the right.

The instrument is used for the following scientific topics: energy research (fuel cells and batteries) (Klages et al., 2013; Manke et al., 2011; Markotter et al., 2012; Totzke et al., 2011); materials research (hydrogen storage materials (Gondek et al., 2011), phase transitions in metals (Woracek et al., 2014) and characterisation of porous media (Hilger et al., 2010)), life science (water uptake in plants and water management in soils) (Matsushima et al., 2009; Totzke et al., 2013), high-TC superconductivity (flux pinning in superconductors) (Kardjilov et al., 2008b), magnetism (visualisation and analysis of magnetic domain networks (Manke et al., 2010) and visualisation of static and alternating magnetic fields), cultural heritage (Salvemini et al., 2015; Triolo et al., 2014) and palaeontology (Grellet-Tinner et al., 2011). In order to accommodate such a broad spectrum of applications new techniques have been developed and implemented, including imaging with polarised neutrons (Kardjilov et al., 2008b), Bragg-edge mapping (Kardjilov et al., 2008a; Woracek et al., 2014), grating interferometry (Manke et al., 2010) and high-resolution neutron imaging (Kardjilov et al., 2011a; Williams et al., 2012).

The beam time at the instrument is provided to the international user community (70%) and to in-house researchers (30%). Short-notice industrial requests are possible by redistributing the beam time schedule. The instrument importance is measured in load factors where the ratio between requested days by external users and the available beam days at the instrument is calculated. The averaged load factor of the CONRAD-2 experiment is approximately 2. A beam time request is submitted as a proposal describing the scientific background and the expected output. Proposals are reviewed by an international panel of noted scientists. Beam time at the instrument is assigned to the proposals obtaining the highest ranking. Proposal rounds are held twice in a year and the beam time for approved proposals is allocated in the next half year. The average number of submitted proposals per half-year period at the CONRAD-2 instrument is 11 requesting in usual 90 days of beam time. The origin of the submitted proposals is distributed as following: 50% from Germany, 25% from EU countries and 25% from countries outside EU (USA, Japan, South Korea, South Africa, etc.).

Results of measurements performed at CONRAD-1 and 2 are usually published in peer-reviewed journals. The instrument is used also for performing work for diploma/master and PhD theses in in-house or external projects. The average number of publications per year is 17 where 2 of them are in form of either diploma or master thesis.

Concerning the beam parameters, instrument infrastructure and scientific output, the CONRAD-2 instrument is comparable with the leading neutron imaging instruments worldwide (Calzada et al., 2009; Hussey et al., 2005; Kaestner et al., 2011).

### 3. Examples of quantification of hydrogen embrittlement in iron sample

The advantages of the upgraded instrument CONRAD-2 were demonstrated in an investigation of hydrogen embrittlement and blistering in electrochemically charged technical iron (Griesche et al., 2014). The low background at the beam line allows for a higher signal-to-noise ratio in the obtained images. The cold neutron beam provides better contrast for the small amount of absorbed hydrogen. Additionally, thin scintillator screens (tens of  $\mu\text{m}$  thick) based on  $\text{Gd}_2\text{O}_2\text{S}$  (Gadox) can be used for high-resolution imaging, which is essential to resolve microcracks filled with molecular hydrogen. For neutron detection, a high-resolution setup with a pixel size of 6.43

$\mu\text{m}$  and field-of-view of  $13\text{ mm} \times 13\text{ mm}$  was used (Williams et al., 2012). The exposure time was 40 s for each image and 2 images per step (integration) were taken. An erosion filter (taking the minimum value of the two images) was applied in order to suppress the large number of white spots in the images. Tomography experiments were performed with 600 projections, giving rise to a total measuring time of  $\sim 12\text{ h}$  per tomogram. An example of a tomographic investigation of technical iron (ARMCOTM) is shown in Fig. 2.

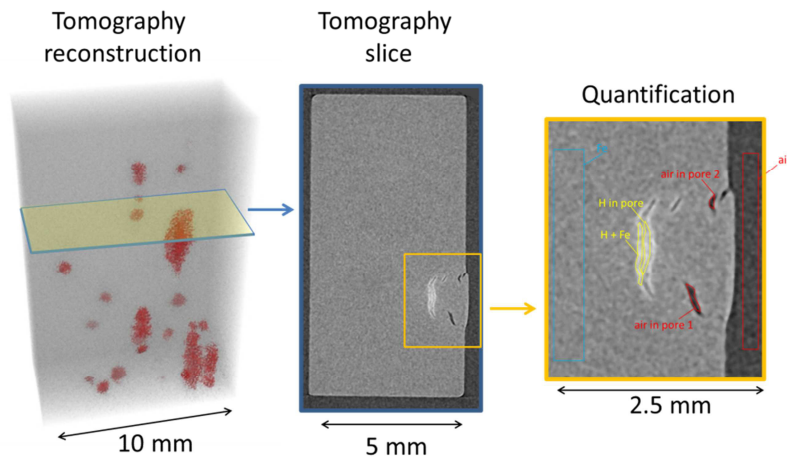


Fig. 2. Example of high-resolution tomography of technical iron (ARMCOTM) charged electrochemically with hydrogen (Griesche et al., 2014). (a) Embrittlement and blistering effects are well visible in the tomography reconstruction. The high-attenuating hydrogen is marked by red colour. (b) Some of the cracks are filled with hydrogen (bright cracks) while the cracks close to the surface are free of hydrogen (dark cracks). Hydrogen diffusion in the area around the cracks is observed too. (c) Regions of interest containing different elements were defined for the quantification procedure.

As shown in Fig. 2 b some of the cracks are bright due to the presence of hydrogen and some of them close to the surface don't contain hydrogen therefore they are dark. It is interesting to mention that the cracks filled by hydrogen have bright edges which is an evidence that some hydrogen is diffused in the material. The explanation of this result by refraction contrast on the crack's edges is inconsistent with the observation that the dark pores don't obey contrast enhanced edges. In addition the tomography investigation of the annealed sample doesn't show any bright cracks due to the hydrogen release at high temperatures (Griesche et al., 2014).

The hydrogen content in the cracks and the iron matrix was quantified. For this purpose the attenuation coefficients in different areas of the tomographic slice shown in Fig 2 c were reconstructed. The results are given in Table 2.

Table 2: Macroscopic attenuation coefficients measured in the ROIs shown in Fig. 2 c

ROI	air	air in pore 1	air in pore 2	Fe	H in pore	H+Fe
$\Sigma, (\text{cm}^{-1})$	0.06	0.00	0.00	0.88	1.57	1.58

The results from Table 2 show some different values for the attenuation coefficient of air in the cracks and the area around the sample. Evidently the two values should be the same. The reason for this discrepancy is the statistical noise in the collected projections which results in some uncertainty of the reconstructed attenuation coefficients in the range of 5-6 %.

The attenuation coefficients  $\Sigma$  in the investigated object can be connected with the density of the corresponding elements:

$$\rho(g/cm^3) = \frac{at.wt.\Sigma}{\sigma_{total}N_a}, \quad (1)$$

where  $\sigma_{total}$  is the total cross section of hydrogen for cold neutrons which is experimentally determined for the imaging beam line CONRAD-2 as 110 barn ( $1 \text{ barn} = 10^{-24} \text{ cm}^2$ ).  $N_a$  is Avogadro's constant  $6.022 \times 10^{23} \text{ mol}^{-1}$ ,  $\rho$  is the density of the element and *at.wt.* its atomic weight. Conversion into  $\text{mol/cm}^3$  can be made by division of the density value through the molar weight for hydrogen (assuming ideal gas behaviour)  $M_H = 2.02 \text{ g/mol}$ . In this way, Eq. (1) yields for the hydrogen in the crack and in the iron matrix as following:

$$\rho_{H\_in\_crack} = \frac{1 \times 1.57}{110 \times 0.6022} \times \frac{1}{2.02} = 0.012 \text{ mol/cm}^3 \quad (2)$$

$$\rho_{H\_in\_Fe} = \frac{1 \times (1.58 - 0.88)}{110 \times 0.6022} \times \frac{1}{2.02} = 0.005 \text{ mol/cm}^3 \quad (3)$$

Using this calculation procedure, the hydrogen concentration can be reconstructed in 3D and quantitative values of the gas pressure in cracks or hydrogen amount in the iron matrix can be obtained. This helps to answer fundamental questions related to hydrogen diffusion in metals as shown in (Griesche et al., 2014).

#### 4. Conclusions

The upgraded neutron instrument CONRAD-2 provides a cold neutron beam for imaging. The high intensity of the beam and its low contamination by fast neutrons and  $\gamma$  photons provide excellent conditions for new experimental techniques such as imaging with monochromatic and polarised neutrons, grating interferometry and high-resolution imaging. The use of cold neutrons increases the sensitivity for hydrogenous materials and allow for, e.g., the quantification of small amounts of hydrogen.

The neutron imaging instrument CONRAD-2 at HZB has a high impact in the neutron user community. Its flexibility and broad spectrum of options attract a large number of users from different research fields – fundamental physics, magnetism, material science, engineering, plant physiology, food science, archaeology and palaeontology.

#### References

- Calzada, E., Gruenauer, F., Muhlbauer, M., Schillinger, B., Schulz, M., 2009. New design for the ANTARES-II facility for neutron imaging at FRM II. *Nucl Instrum Meth A* 605, 50-53.
- Gondek, L., Selvaraj, N.B., Czub, J., Figiel, H., Chapelle, D., Kardjilov, N., Hilger, A., Manke, I., 2011. Imaging of an operating LaNi<sub>4.8</sub>Al<sub>0.2</sub>-based hydrogen storage container. *International Journal of Hydrogen Energy* 36, 9751-9757.
- Grellet-Tinner, G., Sim, C.M., Kim, D.H., Trimby, P., Higa, A., An, S.L., Oh, H.S., Kim, T., Kardjilov, N., 2011. Description of the first lithostrotian titanosaur embryo in ovo with Neutron characterization and implications for lithostrotian Aptian migration and dispersion. *Gondwana Research* 20, 621-629.
- Griesche, A., Dabah, E., Kannengiesser, T., Kardjilov, N., Hilger, A., Manke, I., 2014. Three-dimensional imaging of hydrogen blister in iron with neutron tomography. *Acta Materialia* 78, 14-22.
- Hilger, A., Kardjilov, N., Kandemir, T., Manke, I., Banhart, J., Penumadu, D., Manescu, A., Strobl, M., 2010. Revealing microstructural inhomogeneities with dark-field neutron imaging. *Journal of Applied Physics* 107, 036101.
- Hussey, D.S., Jacobson, D.L., Arif, M., Huffman, P.R., Williams, R.E., Cook, J.C., 2005. New neutron imaging facility at the NIST. *Nucl Instrum Meth A* 542, 9-15.
- Kaestner, A.P., Hartmann, S., Kühne, G., Frei, G., Grünzweig, C., Josic, L., Schmid, F., Lehmann, E.H., 2011. The ICON beamline – A facility for cold neutron imaging at SINQ. *Nuclear Instruments and Methods in Physics Research Section A: Accelerators, Spectrometers, Detectors and Associated Equipment* 659, 387-393.
- Kardjilov, N., Dawson, M., Hilger, A., Manke, I., Strobl, M., Penumadu, D., Kim, K.H., Garcia-Moreno, F., Banhart, J., 2011a. A highly adaptive detector system for high resolution neutron imaging. *Nuclear Instruments and Methods in Physics Research Section A: Accelerators, Spectrometers, Detectors and Associated Equipment* 651, 95-99.

- Kardjilov, N., Hilger, A., Dawson, M., Manke, I., Banhart, J., Strobl, M., Böni, P., 2010. Neutron tomography using an elliptic focusing guide. *Journal of Applied Physics* 108 034905.
- Kardjilov, N., Hilger, A., Manke, I., Garcia-Moreno, F., Banhart, J., 2008a. Bragg-edge Imaging with Neutrons. *Materials Testing-Materials and Components Technology and Application* 50, 569-571.
- Kardjilov, N., Hilger, A., Manke, I., Strobl, M., Dawson, M., Williams, S., Banhart, J., 2011b. Neutron tomography instrument CONRAD at HZB. *Nuclear Instruments and Methods in Physics Research Section A: Accelerators, Spectrometers, Detectors and Associated Equipment* 651, 47-52.
- Kardjilov, N., Manke, I., Strobl, M., Hilger, A., Treimer, W., Meissner, M., Krist, T., Banhart, J., 2008b. Three-dimensional imaging of magnetic fields with polarized neutrons. *Nature Physics* 4, 399-403.
- Kardjilov, N., Manke I., Hilger A., Strobl M., Banhart, J., 2011. Neutron imaging in materials science. *Materials Today* 14, 248-256.
- Klages, M., Enz, S., Markotter, H., Manke, I., Kardjilov, N., Scholta, J., 2013. Investigations on dynamic water transport characteristics in flow field channels using neutron imaging techniques. *Journal of Power Sources* 239, 596-603.
- Manke, I., Kardjilov, N., Schäfer, R., Hilger, A., Strobl, M., Dawson, M., Grünzweig, C., Behr, G., Hentschel, M., David, C., Kupsch, A., Lange, A., Banhart, J., 2010. Three-dimensional imaging of magnetic domains. *Nature Communications* 1, 125, DOI: 110.1038/ncomms1125.
- Manke, I., Kardjilov, N., Strobl, M., Hilger, A., Banhart, J., 2008. Investigation of the skin effect in the bulk of electrical conductors with spin-polarized neutron radiography. *Journal of Applied Physics* 104, 076109.
- Manke, I., Markotter, H., Totzke, C., Kardjilov, N., Grothausmann, R., Dawson, M., Hartnig, C., Haas, S., Thomas, D., Hoell, A., Genzel, C., Banhart, J., 2011. Investigation of Energy-Relevant Materials with Synchrotron X-Rays and Neutrons. *Adv. Eng. Mater.* 13, 712-729.
- Manke, I., Strobl, M., Kardjilov, N., Hilger, A., Treimer, W., Dawson, M., Banhart, J., 2009. Investigation of soot sediments in particulate filters and engine components. *Nuclear Instruments and Methods in Physics Research Section A: Accelerators, Spectrometers, Detectors and Associated Equipment* 610, 622-626.
- Markotter, H., Manke, I., Kuhn, R., Arlt, T., Kardjilov, N., Hentschel, M.P., Kupsch, A., Lange, A., Hartnig, C., Scholta, J., Banhart, J., 2012. Neutron tomographic investigations of water distributions in polymer electrolyte membrane fuel cell stacks. *Journal of Power Sources* 219, 120-125.
- Matsushima, U., Herppich, W.B., Kardjilov, N., Graf, W., Hilger, A., Manke, I., 2009. Estimation of water flow velocity in small plants using cold neutron imaging with D2O tracer. *Nuclear Instruments and Methods in Physics Research Section A: Accelerators, Spectrometers, Detectors and Associated Equipment* 605, 146-149.
- Salvemini, F., Grazzi, F., Kardjilov, N., Manke, I., Civita, F., Zoppi, M., 2015. Neutron computed laminography on ancient metal artefacts. *Analytical Methods*.
- Schroder, A., Wippermann, K., Arlt, T., Sanders, T., Baumhofer, T., Kardjilov, N., Mergel, J., Lehnert, W., Stolten, D., Banhart, J., Manke, I., 2013. In-plane neutron radiography for studying the influence of surface treatment and design of cathode flow fields in direct methanol fuel cells. *International Journal of Hydrogen Energy* 38, 2443-2454.
- Strobl, M., Grünzweig, C., Hilger, A., Manke, I., Kardjilov, N., David, C., Pfeiffer, F., 2008. Neutron Dark-Field Tomography. *Phys Rev Lett* 101, 123902.
- Strobl, M., Manke, I., Kardjilov, N., Hilger, A., Dawson, M., Banhart, J., 2009. Advances in neutron radiography and tomography. *Journal of Physics D-Applied Physics* 42, 243001.
- Tötzke, C., Manke, I., Arlt, T., Markotter, H., Kardjilov, N., Hilger, A., Williams, S.H., Kruger, P., Kuhn, R., Hartnig, C., Scholta, J., Banhart, J., 2012. Investigation of fuel cells using scanning neutron imaging and a focusing neutron guide. *Nucl Instrum Meth A* 663, 48-54.
- Tötzke, C., Manke, I., Hilger, A., Choinka, G., Kardjilov, N., Arlt, T., Markotter, H., Schroder, A., Wippermann, K., Stolten, D., Hartnig, C., Kruger, P., Kuhn, R., Banhart, J., 2011. Large area high resolution neutron imaging detector for fuel cell research. *Journal of Power Sources* 196, 4631-4637.
- Tötzke, C., Miranda, T., Konrad, W., Gout, J., Kardjilov, N., Dawson, M., Manke, I., Roth-Nebelsick, A., 2013. Visualization of embolism formation in the xylem of liana stems using neutron radiography. *Annals of Botany* 111, 723-730.
- Triolo, R., Lo Celso, F., Tisseyre, P., Kardjilov, N., Wieder, F., Hilger, A., Manke, I., 2014. Neutron tomography of ancient lead artefacts. *Analytical Methods* 6, 2390-2394.
- Williams, S.H., Hilger, A., Kardjilov, N., Manke, I., Strobl, M., Douissard, P.A., Martin, T., Riesemeier, H., Banhart, J., 2012. Detection system for microimaging with neutrons. *Journal of Instrumentation* 7, P02014.
- Woracek, R., Penumadu, D., Kardjilov, N., Hilger, A., Boin, M., Banhart, J., Manke, I., 2014. 3D Mapping of Crystallographic Phase Distribution using Energy-Selective Neutron Tomography. *Advanced Materials* 26, 4069-4073.
- Woracek, R., Penumadu, D., Kardjilov, N., Hilger, A., Strobl, M., Wimpory, R.C., Manke, I., Banhart, J., 2011. Neutron Bragg-edge-imaging for strain mapping under in situ tensile loading. *Journal of Applied Physics* 109, 093506.